AGU PUBLICATIONS

Geophysical Research Letters

RESEARCH LETTER
10.1002/2013GL058236

Key Points:
- Strong Alpine Fault gouges exhibit potentially unstable behavior
- Alpine Fault gouge strength and stability are temperature-dependent
- An elevated geothermal gradient promotes rate-weakening

Supporting Information:
- Readme
- Text S1
- Text S2

Correspondence to:
C. Boulton,
carolyn.boulton@pg.canterbury.ac.nz

Citation:
Boulton, C., D. E. Moore, D. A. Lockner, V. G. Toy, J. Townend, and R. Sutherland (2014), Frictional properties of exhumed fault gouges in DFDP-1 cores, Alpine Fault, New Zealand, *Geophys. Res. Lett.*, *41*, doi:10.1002/2013GL058236.

Received 10 OCT 2013
Accepted 27 DEC 2013
Accepted article online 3 JAN 2014

Frictional properties of exhumed fault gouges in DFDP-1 cores, Alpine Fault, New Zealand

Carolyn Boulton[1], Diane E. Moore[2], David A. Lockner[2], Virginia G. Toy[3], John Townend[4], and Rupert Sutherland[5]

[1]Department of Geological Sciences, University of Canterbury, Christchurch, New Zealand, [2]U.S. Geological Survey, Menlo Park, California, USA, [3]Department of Geology, University of Otago, Dunedin, New Zealand, [4]School of Geography, Environment, and Earth Sciences, Victoria University of Wellington, Wellington, New Zealand, [5]GNS Science, Lower Hutt, New Zealand

Abstract Principal slip zone gouges recovered during the Deep Fault Drilling Project (DFDP-1), Alpine Fault, New Zealand, were deformed in triaxial friction experiments at temperatures, T, of up to 350°C, effective normal stresses, σ_n', of up to 156 MPa, and velocities between 0.01 and 3 μm/s. Chlorite/white mica-bearing DFDP-1A blue gouge, 90.62 m sample depth, is frictionally strong (friction coefficient, μ, 0.61–0.76) across all experimental conditions tested (T = 70–350°C, σ_n' = 31.2–156 MPa); it undergoes a transition from positive to negative rate dependence as T increases past 210°C. The friction coefficient of smectite-bearing DFDP-1B brown gouge, 128.42 m sample depth, increases from 0.49 to 0.74 with increasing temperature and pressure (T = 70–210°C, σ_n' = 31.2–93.6 MPa); the positive to negative rate dependence transition occurs as T increases past 140°C. These measurements indicate that, in the absence of elevated pore fluid pressures, DFDP-1 gouges are frictionally strong under conditions representative of the seismogenic crust.

1. Introduction

The Alpine Fault represents the largest onshore seismic hazard in New Zealand, accommodates 65–75% of the total relative Australia-Pacific plate boundary motion, ruptures episodically in large magnitude ($M_w \sim 8$) earthquakes, and is late in its seismic cycle (last event 1717 AD; recurrence interval 329 ± 68 years) [*Sutherland et al.*, 2007; *Berryman et al.*, 2012]. On the central Alpine Fault, between the Wanganui and Waiho (Franz Josef) Rivers, rapid exhumation of amphibolite-facies mylonites from c. 35 km depth in the past 5–8 Myr has resulted in a high shallow geothermal gradient of 62.6 ± 2.1°C/km [e.g., *Norris and Cooper*, 2007; *Sutherland et al.*, 2007, 2012]. Because the central Alpine Fault exhumes its hanging wall, the mineralogical, microstructural, and frictional properties of principal slip zone (PSZ) materials may be diagnostic of similar materials currently deforming at depth [*Townend et al.*, 2009].

Understanding the geological, geophysical, hydrological, and seismological properties of the Alpine Fault are aims of the Deep Fault Drilling Project (DFDP). The first phase of the Deep Fault Drilling Project (DFDP-1) successfully constructed two shallow boreholes intersecting the fault (DFDP-1A, 96.6 m and DFDP-1B, 150.4 m) at Gaunt Creek and collected rock cores, wireline logging data, and hydraulic measurements spanning the fault zone (Figure 1). Initial DFDP publications have highlighted the important role fluid-rock interactions, which result in phyllosilicate precipitation and calcite mineralization, may play in modulating the mechanical properties of the Alpine Fault [*Sutherland et al.*, 2012; *Townend et al.*, 2013].

Norris and Cooper [2007] found that central Alpine Fault gouges and cataclasites form from mechano-chemical alteration of primarily Pacific-plate Alpine Schist-derived mylonites, which are continuous for ~150 km along-strike. *Warr and Cox* [2001] documented two main phases of alteration in Gaunt Creek surface-outcrop fault gouges and cataclasites: (1) hydrous chloritization at temperatures less than 320°C, and (2) growth of swelling clays, particularly smectite, at temperatures less than 120°C. The extent to which alteration processes affect the frictional strength and frictional stability of central Alpine Fault gouges remains incompletely understood. Here, we report the results of low-velocity hydrothermal friction experiments designed to investigate the conditions requisite for earthquake rupture nucleation. Experiments were conducted on two fault gouges comprising the principal slip zone intersected in DFDP-1A and DFDP-1B. Because each PSZ gouge has a distinct mineral

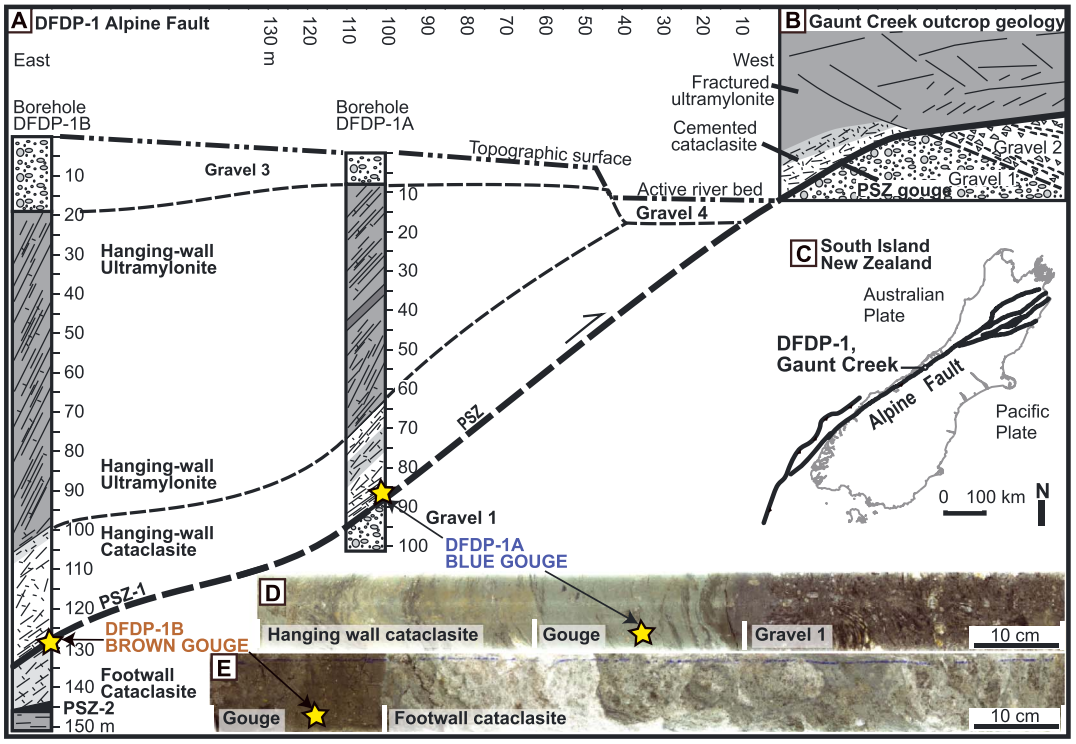

Figure 1. Location map and materials used in hydrothermal friction experiments. (a) Lithological cross sections of the two boreholes drilled during Phase 1 of the Deep Fault Drilling Project (DFDP-1), Alpine Fault, at Gaunt Creek. Horizontal axis (distance between boreholes) located across the top of figure. Samples were collected from the depths designated with stars. (b) A schematic cross section of prominent fault scarp outcrop geology on the south side of Gaunt Creek. (c) The Australia-Pacific plate boundary in the South Island of New Zealand. (d) 180° scan of DFDP-1A Run 66, section 1, from which 1A blue gouge was sampled. (e) 180° scan of DFDP-1B Run 59, section 1, from which 1B brown gouge was sampled. Figure modified from *Sutherland et al.* [2012].

assemblage representative of high or low temperature alteration, experimental results quantify how frictional properties vary with mineralogy, temperature, and pressure.

2. Materials Studied

DFDP-1 principal slip zone (PSZ) materials occur within a wider alteration zone characterized by cataclastic deformation and precipitation of phyllosilicates and carbonates [*Sutherland et al.*, 2012; *Townend et al.*, 2013] (Figure 1). Two random-fabric PSZ fault gouges (incohesive fault rock with >90% matrix grains <0.1 mm in size) were selected from DFDP-1A and DFDP-1B cores for investigation: (1) a blue fault gouge from DFDP-1A (Run 66, section 1, 0.44 m below top of core, 90.62 m adjusted hole depth; hereafter "1A blue gouge") and (2) a brown fault gouge from DFDP-1B (Run 59, section 1, 0.12 m below top of core, 128.42 m adjusted hole depth; hereafter "1B brown gouge").

For the hydrothermal friction experiments, gouge samples were vacuum dried overnight at 40°C and then gently disaggregated using a mortar and pestle. Sieved separates (<150 μm) were made by passing each gouge powder through a 100# sieve. Quantitative X-ray diffraction (XRD) was done on the sieved gouge separates following methods described by *Boulton et al.* [2012]. Particle size analysis of each separate was undertaken with a Saturn Digisizer 5205 following the method of *Storti and Balsamo* [2010].

The c. 18 cm thick 1A blue gouge forms a gradational upper contact with foliated cataclasite and a sharp, but undulating (cm- to mm-scale), lower contact with c. 2 cm thick brown gouge. It contains calcite vein fragments and clasts of ultramylonite, cataclasite, and the underlying brown gouge. The sieved separate contains the following minerals: quartz (29%), K feldspar (42%), plagioclase (6%), calcite (7%), muscovite/illite (9%), chlorite (clinochlore) (7%), anatase (<1%), and rare pyrite. Median grain size is c. 4 μm, with 90% of analyzed grains having diameters <65 μm.

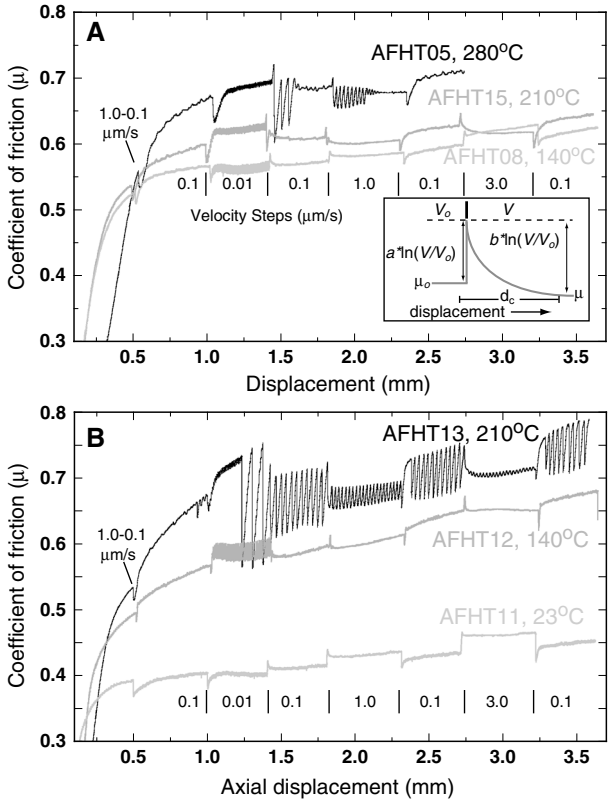

Figure 2. Plots of coefficient of friction vs. axial displacement for triaxial experiments conducted on Alpine Fault gouges. For a 30° inclined saw cut, fault-parallel displacement is approximately 15% larger than axial displacement. (a) Representative DFDP-1A blue gouge experiments conducted following depth-dependent increases in temperature and effective normal stress. Rate and state friction parameters are depicted graphically in the inset figure. (b) Representative DFDP-1B brown gouge experiments conducted following the same method. Velocity steps are demarcated.

The upper contact of the c. 20 cm thick 1B brown gouge was not recovered, but this material is compositionally similar to the brown gouge that occurs below the 1A blue gouge. Compared to the 1A blue gouge, 1B brown gouge has a higher proportion of brown gouge clasts, fewer cataclasite and ultramylonite clasts, fewer calcite vein fragments, and Fe oxide-hydroxide cement. The sieved separate contains the following minerals: quartz (22%), K feldspar (15%), plagioclase (21%), calcite (10%), muscovite/illite (5%), smectite (montmorillonite) (26%), chlorite (clinochlore) (1%), and rare pyrite. The 1B brown gouge median grain size is c. 3 μm, with 90% of analyzed grains having diameters $<$41 μm; thus, it is finer grained than the 1A blue gouge.

3. Hydrothermal Friction Experiments

3.1. Experimental Procedure

A total of 18 shearing experiments were conducted using a triaxial deformation apparatus: 10 experiments following a lithostatic confining pressure gradient consistent with crustal density of 2650 kg/m^3, hydrostatic pore fluid pressure, and a 35°C/km geothermal gradient. A geothermal gradient of 35°C/km was chosen to coincide with seismological observations of microseismicity in the hanging wall of the Alpine Fault extending to 10 ± 2 km depth [*Boese et al.*, 2012], consistent with available geological data [*Toy et al.*, 2010]. Although the shallow geothermal gradient on the Alpine Fault is high, a depth-averaged geothermal gradient of 35°C/km is appropriate if the onset of quartz plasticity at approximately 350°C represents the base of the brittle seismogenic crust [e.g., *Scholz*, 1998].

To explore how elevated temperatures might affect frictional properties, six experiments were conducted to simulate higher crustal temperatures at effective normal stresses between 31.2 and 93.6 MPa. The remaining two experiments were conducted at room temperature and an effective normal stress of 31.2 MPa to provide

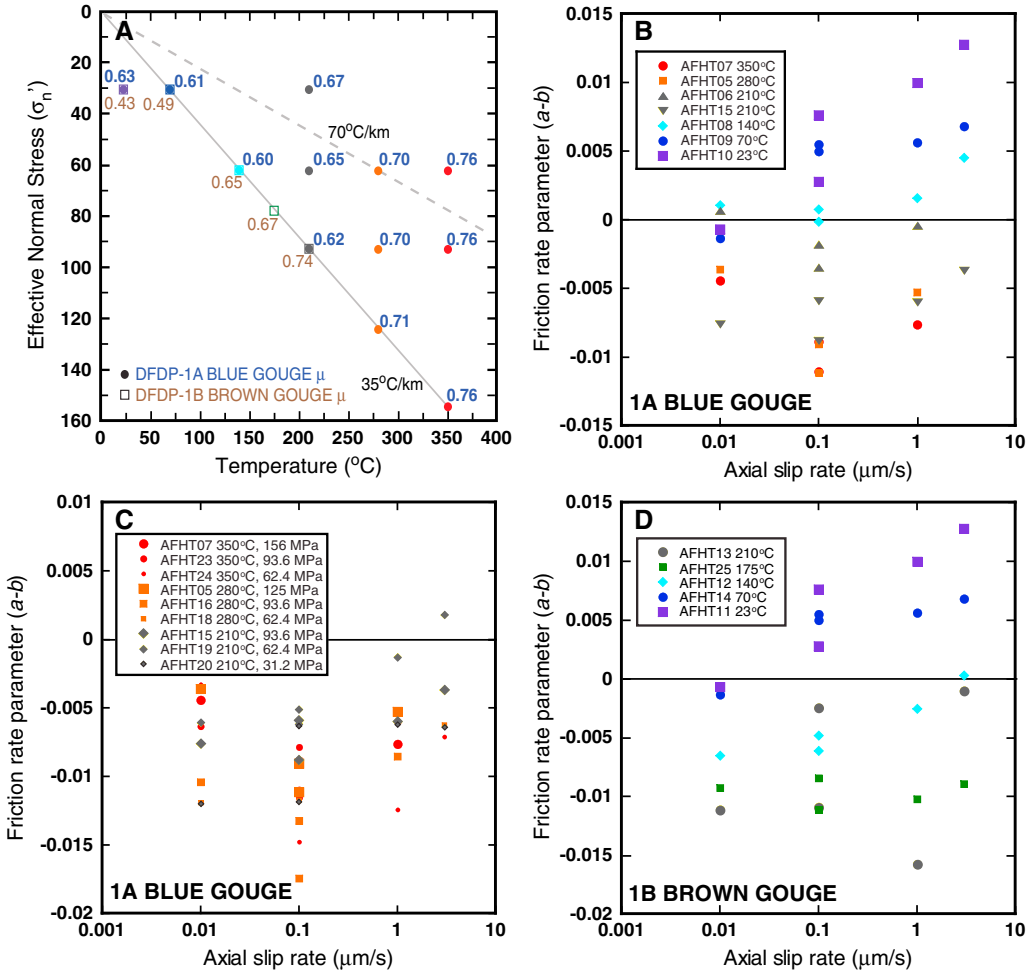

Figure 3. Summary plots of experimental results. (a) Frictional strength as a function of gouge lithology, temperature, and effective normal stress. DFDP-1A blue gouge μ values are in blue font, and DFDP-1B brown gouge μ values are in brown font. 1A blue gouge symbols (circles) and 1B brown gouge symbols (open squares) are color coded to match temperature in plots b, c, and d. Typical uncertainties in μ for tests from room temperature to 210° (using Pb jackets) are ±0.02; uncertainties at higher temperatures (with Cu jackets) are ±0.03. Plotted for reference are σ_n'-T curves approximating in situ conditions for 35°C/km and 70°C/km geothermal gradients. (b) DFDP-1A blue gouge friction rate parameters. (c) Results from more detailed experiments on 1A blue gouge investigating the competing effects of temperature and pressure on frictional stability. (d) DFDP-1B brown gouge friction rate parameters. The standard deviation in a, b_1, b_2, and $(a–b)$ is in the order of 10^{-4}. All data are tabulated in supporting information.

data comparable with those of previous experiments on surface-outcrop gouges [*Boulton et al.*, 2012]. The 1A blue gouge was tested at temperatures up to 350°C; these temperatures are within the thermodynamic stability range of chlorite and muscovite/illite. Experiments on the 1B brown gouge were conducted at temperatures up to 210°C, somewhat in excess of the thermodynamic stability range of smectite [*Pytte and Reynolds*, 1989].

Experiments were conducted using an inclined (30° plane) saw cut configuration, furnace assembly, and methods described in *Moore and Lockner* [2011]. To determine the rate dependence of friction, velocity steps of 0.01–3 μm/s were imposed. Total axial displacement varied between 2.41 and 3.63 mm (Figure 2). For a 30° inclined saw cut, fault-parallel displacement is approximately 15% larger than axial displacement. Supporting information contains full experimental methods, data processing details, and a table of all experiments conducted.

3.2. Data Analysis

We present strength results in terms of the coefficient of friction, $\mu = \tau/\sigma_n'$ where τ is the resolved shear stress, $\sigma_n' = \sigma_n - P_p$ is the effective normal stress, and σ_n and P_p are the resolved normal stress and the pore pressure, respectively. Because many of the samples experienced strain hardening, nearly all of the reported friction

coefficients (Figure 3a) were measured at 2.70 mm axial displacement and 0.1 μm/s velocity. Two samples (AFHT16 and AFHT23) underwent early jacket failure; in those cases, the reported value of μ was measured near the beginning of the 0.1 μm/s velocity step (2.39 mm axial displacement).

In terms of rate and state friction equations, linear stability analysis shows that the mechanical conditions and constitutive properties that distinguish stable (aseismic) from unstable (seismic) sliding can be quantified by a friction rate parameter (a–b) and a critical slip distance d_c [*Dieterich*, 1979; *Ruina*, 1983]. We estimated (a–b) and other constitutive parameters using an iterative least squares method incorporating the *Dieterich* [1979] constitutive friction equation

$$\mu_{ss} = \mu_0 + a \ln\left(\frac{V}{V_0}\right) + b_1 \ln\left(\frac{V_0\theta_1}{d_{c1}}\right) + b_2 \ln\left(\frac{V_0\theta_2}{d_{c2}}\right) \quad (1)$$

where V_0 and V are the initial and final load point velocities, respectively, μ_0 and μ_{ss} are the initial and final, steady-state, coefficients of friction, a, b_1, b_2, d_{c1}, and d_{c2} are empirical constants, and θ_1 and θ_2 are state variables that evolve with time according to

$$\frac{d\theta_i}{dt} - 1 - \frac{V\theta_i}{d_{ci}}, (i = 1, 2) \quad (2)$$

For many velocity steps, data are well fit using a single state variable, and $\theta_2 = 0$ (equation (1)). In the two state variable models, a–b was determined by letting $b = b_1 + b_2$. Within the rate and state framework, frictional sliding will be unstable, or potentially unstable, when a–$b \leq 0$. Frictional sliding will be stable when a–$b > 0$. The stability criterion also requires that the elastic stiffness, k, of the loading system be smaller than the critical stiffness, k_c, which is defined by the frictional properties of the slipping fault [*Ruina*, 1983; *Scholz*, 1998]. Constitutive parameters for the least squares fit of all modeled velocity steps are tabulated in the supporting information.

3.3. Results

The friction coefficient of the 1A blue gouge increased from $\mu = 0.61$ at low effective normal stress and temperature ($\sigma_n' = 31.2$ MPa and $T = 70$°C) to $\mu = 0.76$ at higher effective normal stress and temperature ($\sigma_n' = 156$ MPa and $T = 350$°C). As seen in Figure 3a, the 1A blue gouge friction coefficient depends primarily on temperature and has little sensitivity to σ_n', especially above 250°C. We observed a rapid increase in the 1B brown gouge friction coefficient, from $\mu = 0.49$ at low effective normal stress and temperature ($\sigma_n' = 31.2$ MPa and $T = 70$°C) to $\mu = 0.74$ at higher effective normal stress and temperature ($\sigma_n' = 93.6$ MPa and $T = 210$°C; Figures 2 and 3).

1A blue gouge exhibited near zero or positive (a–b) for all velocity steps conducted at $T \leq 140$°C, $\sigma_n' \leq 62.4$ MPa (Figures 2a and 3b). In experiments conducted at temperatures ≥210°C, values of (a–b) were negative for all velocities and all effective normal stresses (Figures 3b and 3c). We observed one exception at 210°C, $\sigma_n' = 62.4$, $v = 3$ μm/s, where (a–b) was positive (Figure 4c). The friction rate parameter, (a–b), of 1B brown gouge, was near zero or positive at 23°C and 70°C. At 140°C, $\sigma_n' = 62.4$ MPa, values of (a–b) were negative for every velocity step size, becoming less negative with increasing velocity. At 175°C, $\sigma_n' = 62.4$ MPa, and at 210°C, $\sigma_n' = 93.6$ MPa, all measured values of (a–b) were negative (Figure 3d).

4. Discussion

In hydrothermal experiments conducted under conditions approximating those expected for a 35°C/km geothermal gradient to a depth of 10 km, 1A blue gouge underwent a transition from positive to negative (a–b) as temperature increased past 210°C. A similar transition to rate-weakening behavior at elevated temperatures also occurred in low velocity hydrothermal friction experiments on granite gouges ($T = 100$–350°C) [*Blanpied et al.*, 1995], illite-rich San Andreas Fault gouges ($T = 266$–349°C) [*Tembe et al.*, 2009], and quartz-illite gouges ($T = 250$–400°C) [*Den Hartog and Spiers*, 2013]. The frictional stability transition observed in the 1A blue gouge at 210°C can be interpreted in the context of microphysical models for quartz-phyllosilicate gouges developed by *Den Hartog and Spiers* [2013] following *Niemeijer and Spiers* [2007].

In those microphysical models, shear deformation is accommodated by dilational granular flow with interchanging framework silicate contacts and frictional slip on phyllosilicates. At steady state, dilation is balanced by solution-assisted compaction and gouge porosity remains low. During a velocity step, dilation accompanies frictional slip along the grain contacts. If the dilation (increase in porosity) that accompanies a velocity increase is greater than the compaction (decrease in porosity) that accompanies sliding at the higher velocity, gouge steady-state frictional strength decreases after a velocity step. According to this interpretation, variations in gouge porosity underpin rate-weakening behavior.

The microphysical models suggest that negative (a–b) is linked to temperature-, grain size-, effective normal stress-, and time-dependent solution-transfer processes that increase grain contact area. These thermally activated processes result in negative (a–b) at temperatures greater than c. 150–250°C and less than c. 350–600°C, depending on sliding velocity and the ratio of phyllosilicate minerals to quartz. At lower temperatures, higher sliding velocities, and/or higher ratios of phyllosilicate minerals to quartz, increases in grain contact area associated with solution-assisted compaction are slow and shear deformation is accommodated primarily by rate-strengthening frictional sliding along grain contacts [*Niemeijer and Spiers*, 2007; *Den Hartog and Spiers*, 2013]. From these microphysical models, it follows that increasing the modal abundance of insoluble, thermodynamically stable, phyllosilicate minerals (e.g., a Gaunt Creek surface-outcrop PSZ gouge had 41% chlorite-muscovite/illite in *Boulton et al*. [2012]) would increase the temperature at which the transition from positive to negative (a–b) occurs.

Our observation of an increase in the 1B brown gouge friction coefficient coincident with rate-weakening behavior agrees with previous findings correlating conditionally unstable or unstable (seismic) slip with frictionally strong materials [*Beeler*, 2007; *Ikari et al*., 2011]. The change from positive to negative rate dependence occurred in the temperature range associated with the thermally driven dehydration of smectite to illite (T = 120–150°C) [*Pytte and Reynolds*, 1989], which may accelerate solution-assisted compaction and/or promote strain localization, both of which are associated with frictional instability [e.g., *Niemeijer and Spiers*, 2007; *Saffer et al*., 2012; *Den Hartog and Spiers*, 2013]. However, the smectite-to-illite reaction is unlikely to have progressed to completion during an ~18.5 h experiment, and the increase in the 1B brown gouge friction coefficient remains the focus of future study. Smectite is a low temperature alteration product of precursor chlorite and muscovite/illite minerals [*Warr and Cox*, 2001; *Boulton et al*., 2012]; therefore, gouges similar to the 1B brown gouge are unlikely to affect central Alpine Fault frictional properties at depths greater than c. 2–3 km given the high shallow geothermal gradient.

High-velocity friction experiments indicate that sliding at coseismic slip rates (~1 m/s) activates dynamic weakening mechanisms that result in very low friction coefficients (μ = 0.2–0.4) [e.g., *Di Toro et al*., 2011]. Whether an earthquake rupture tip can provide the acceleration needed to activate dynamic weakening mechanisms is strongly influenced by the areal distribution of rate-weakening and rate-strengthening materials on the fault plane [e.g., *Noda et al*., 2009; *Kaneko et al*., 2010]. Indeed, frictional failure of the Alpine Fault requires the presence of rate-weakening material as well as sufficient resolved shear stress to overcome its frictional strength. If, as our hydrothermal friction results indicate, earthquake rupture nucleation occurs in frictionally strong, rate-weakening Alpine Fault gouge, determining the stress tensor, pore fluid pressure, and fault geometry at depth is critically important to understanding nucleation processes [e.g., *Wannamaker et al*., 2002; *Boese et al*., 2012; *Barth et al*., 2012].

5. Conclusions

The coefficient of friction of DFDP-1A blue gouge increases with temperature and pressure from μ = 0.61 to μ = 0.76. The transition from positive to negative (a–b) occurs in 1A blue gouge at 210°C, irrespective of effective normal stress in the range tested (σ_n' = 31.2 to 93.6 MPa). The friction coefficient of DFDP-1B brown gouge increases markedly from μ = 0.49 at T = 70°C and σ_n' = 31.2 MPa to μ = 0.65 at T = 140°C and σ_n' = 62.4 MPa, coincident with the transition from positive to negative rate dependence. Our 1B brown gouge data indicate that smectite precipitation promotes rate-strengthening behavior in the shallowest part of the Alpine Fault (uppermost c. 3–4 km for a geothermal gradient of 35°C/km). For the same geothermal gradient, in the depth range c. 6–10 km, the chlorite/white mica-bearing 1A blue gouge exhibits rate-weakening behavior conducive to earthquake rupture nucleation.

Acknowledgments
Mark Raven, Brent Pooley, Rob Spiers, and Lee-Gray Boze provided expert technical assistance. Rate and state friction models were done with XLook. Drilling operations were made possible by Horizon Drilling, Alex Pyne, New Zealand Department of Conservation, Whataroa Community, GNS Science, Deutsche Forschungsgemeinschaft, National Environment Research Council grant NE/H012486/1, the Marsden Fund, and the following universities: Victoria University of Wellington, Otago, Auckland, Canterbury, Bremen, and Liverpool. The manuscript benefited from discussions with C. Boese and reviews by N. Beeler, B. Kilgore, Åke Fagereng, and an anonymous reviewer. Marsden Grant UOO0919 to V. Toy and the U.S. National Earthquake Hazards Reduction Program supported laboratory research.

The Editor thanks Åke Fagereng and an anonymous reviewer for assistance evaluating this manuscript.

References

Barth, N. C., V. G. Toy, R. M. Langridge, and R. J. Norris (2012), Scale dependence of oblique plate-boundary partitioning: New insights from LiDAR, central Alpine fault, New Zealand, *Lithosphere*, doi:10.1130/L201.1.

Beeler, N. M. (2007), Laboratory-observed faulting in intrinsically and apparently weak materials, in *The Seismogenic Zone of Subduction Thrust Faults*, edited by T. H. Dixon and J. C. Moore, pp. 370–449, Columbia University Press, New York.

Berryman, K. B., U. A. Cochran, K. J. Clark, G. P. Biasi, R. M. Langridge, and P. Villamor (2012), Major earthquakes occur regularly on an isolated plate boundary fault, *Science*, *29*(336), 1690–1693, doi:10.1126/science.1218959.

Blanpied, M. L., D. A. Lockner, and J. D. Byerlee (1995), Frictional slip of granite at hydrothermal conditions, *J. Geophys. Res.*, *100*(B7), 13,405–13,064.

Boese, C. M., J. Townend, E. Smith, and T. Stern (2012), Microseismicity and stress in the vicinity of the Alpine Fault, central Southern Alps, New Zealand, *J. Geophys. Res.*, *117*, B02302, doi:10.1029/2011JB008460.

Boulton, C., B. M. Carpenter, V. Toy, and C. Marone (2012), Physical properties of surface outcrop cataclastic fault rocks, Alpine Fault, New Zealand, *Geochem. Geophys. Geosys.*, *13*, Q01018, doi:10.1029/2011GC003872.

Den Hartog, S. A. M., and C. J. Spiers (2013), Influence of subduction zone conditions and gouge composition on frictional slip stability of megathrust fault, *Tectonophysics*, *600*, 75–90, doi:10.1016/j.tecto.2012.11.006.

Di Toro, G., R. Han, T. Hirose, N. De Paola, S. Nielsen, K. Mizoguchi, F. Ferri, M. Cocco, and T. Shimamoto (2011), Fault lubrication during earthquakes, *Nature*, *471*, 494–499, doi:10.1038/nature09838.

Dieterich, J. H. (1979), Modeling of rock friction 1. Experimental results and constitutive equations, *J. Geophys. Res.*, *84*(B5), 2162–2168, doi:10.1029/JB084iB05p02151.

Ikari, M. J., C. Marone, and D. M. Saffer (2011), On the relation between fault strength and frictional stability, *Geology*, *39*(1), 83–86.

Kaneko, Y., J.-P. Avouac, and N. Lapusta (2010), Towards inferring earthquake patterns from geodetic observations of interseismic coupling, *Nat. Geosci.*, *3*, 363–369, doi:10.1038/NGEO843.

Moore, D. E., and D. A. Lockner (2011), Frictional strengths of talc-serpentine and talc-quartz mixtures, *J. Geophys. Res.*, *116*, B01403, doi:10.1029/2010JB007881.

Niemeijer, A. R., and C. J. Spiers (2007), A microphysical model for strong velocity weakening in phyllosilicate-bearing fault gouges, *J. Geophys. Res.*, *112*, BI0405, doi:10.1029/2007JB005008.

Noda, H., E. M. Dunham, and J. R. Rice (2009), Earthquake ruptures with thermal weakening and the operation of major faults at low overall stress levels, *J. Geophys. Res.*, *114*, B07302, doi:10.1029/2008JB006143.

Norris, R. J., and A. F. Cooper (2007), The Alpine Fault, New Zealand: Surface geology and field relationships, in *A Continental Plate Boundary: Tectonics at South Island, New Zealand*, *Geophys. Monogr. Ser.*, vol. 175, edited by D. Okaya, T. Stern, and F. Davey, pp. 159–178, AGU, Washington, D. C.

Pytte, A. M., and R. C. Reynolds (1989), The thermal transformation of smectite to illite, in *Thermal Histories of Sedimentary Basins*, edited by T. H. McCulloh and N. D. Naeser, pp. 133–140, Springer, New York.

Ruina, A. L. (1983), Slip instability and state variable friction laws, *J. Geophys. Res.*, *88*(B12), 10,359–10,370, doi:10.1029/JB088iB12pl10359.

Saffer, D. M., D. A. Lockner, and A. McKiernan (2012), Effects of smectite to illite transformation on the frictional strength and sliding stability of intact marine mudstones, *Geophys. Res. Lett.*, *39*, L11304, doi:10.1029/2012GL051761.

Scholz, C. H. (1998), Earthquakes and friction laws, *Nature*, *391*, 37–42.

Storti, F., and F. Balsamo (2010), Particle size distributions by laser diffraction: Sensitivity of granular matter strength to analytical operating procedures, *Solid Earth*, *1*, 25–48.

Sutherland, R., et al. (2007), Do great earthquakes occur on the Alpine fault in central South Island, New Zealand?, in *A Continental Plate Boundary: Tectonics at South Island, New Zealand*, *Geophys. Monogr. Ser.*, vol. 175, edited by D. Okaya, T. Stern, and F. Davey, 235–251, AGU, Washington, D. C.

Sutherland, R., et al. (2012), Drilling reveals fluid control on architecture and rupture of the Alpine Fault, New Zealand, *Geology*, *40*, 1143–1146, doi:10.1130/G33614.1.

Tembe, S., D. A. Lockner, and T.-F. Wong (2009), Constraints on the stress state of the San Andreas Fault with analysis based on core and cuttings from San Andreas Fault Observatory at Depth (SAFOD) drilling phases 1 and 2, *J. Geophys. Res.*, *114*, B11401, doi:10.1029/2008JB005883.

Townend, J., R. Sutherland, and V. Toy (2009), Deep Fault Drilling Project-Alpine Fault, New Zealand, *Sci. Drill.*, *8*, 75–82.

Townend, J., R. Sutherland, V. G. Toy, J. D. Eccles, C. J. Boulton, S. C. Cox, and D. McNamara (2013), Late-interseismic state of a continental plate-bounding fault: Petrophysical results from DFDP-1 wireline and core analysis, Alpine fault, New Zealand, *Geochem. Geophys. Geosyst.*, *14*, 3801–3820, doi:10.1002/ggge/20236.

Toy, V. G., D. Craw, A. F. Cooper, and R. J. Norris (2010), Thermal regime in the central Alpine Fault zone, New Zealand: Constraints from microstructures, biotite chemistry and fluid inclusion data, *Tectonophysics*, *485*, 178–192, doi:10.1016/j.tecto.2009.12.013.

Wannamaker, P. E., G. R. Jiracek, J. A. Stodt, T. G. Caldwell, V. M. Gonzalez, J. D. McKnight, and A. D. Porter (2002), Fluid generation and pathways beneath an active compressional orogen, the New Zealand Southern Alps, inferred from magnetotelluric data, *J. Geophys. Res.*, *107*(B6), doi:10.1029/2001JB000186.

Warr, L. N., and S. Cox (2001), Clay mineral transformations and weakening mechanisms along the Alpine Fault, New Zealand, in *The Nature and Tectonic Significance of Fault Zone Weakening*, Spec. Pub., vol. 186, edited by R. E. Holdsworth et al., pp. 85–101, Geol. Soc. London, London.